

Waveguide Ports: Five Examples Using XFDTD[®] EM Simulation Software

Example 1: Slotted Waveguide Antenna

Summary: A composite right/left-handed waveguide with irregularly spaced and rotated slots is used as an antenna.

Example 2: Waveguide Cross-Coupled Filter Simulation

Summary: Waveguide ports are used to excite a complex microwave filter with a folded waveguide structure linked by a cross-coupled filter.

Example 3: Wideband Pseudo-Elliptic Waveguide Filter

Summary: Waveguide ports are used to excite a microwave filter constructed from WR-90 waveguide with cavity-backed inverters and multiple irises.

Example 4: Rectangular Waveguide Mode Converters

Summary: This example investigates higher order modes available in waveguide ports in XFDTD. Here rectangular waveguides of WR187 size (47.55 x 22.15 mm) are used to create mode converters by introducing double or triple bends.

Example 5: Microstrip Gap Waveguide on Electronic Band Gap Substrate

Summary: A microstrip gap waveguide is simulated over a mushroom-type electronic band gap (EBG) surface to demonstrate the effectiveness of the design.

[Next Page](#)

Example 1: Slotted Waveguide Antenna

Summary: A composite right/left-handed waveguide with irregularly spaced and rotated slots is used as an antenna.

This example demonstrates a complex antenna comprised of a composite right/left-handed (CRLH) waveguide and unequally spaced slots [1]. The antenna is fed by a WR-90 waveguide that enters at the bottom of the device. After the input port, a matching transition region modifies the fields for propagation down the CRLH waveguide. The CRLH waveguide has numerous equally-spaced unit cells which each contain small apertures for field propagation. The radiation is through six tilted slots in the top plate of the waveguide. The spacing between the slots and the tilt angle of each slot varies.

The CAD-based geometry in XFDTD is shown in Figure 1 where the input port is to the left and bottom and the CRLH waveguide extends to the right. The slots are visible in the top of the structure of Figure 1. A more detailed view of the slots is shown in Figure 2, where the XFDTD mesh is also visible. Due to the complex nature of the slots which are not aligned with the FDTD grid, the XACT Accurate Cell Technology meshing feature is used to precisely mesh the slot dimensions and orientation. In Figure 3, the input port at the bottom of the waveguide is shown with the applied TE_{10} mode. A cut-away mesh view of the interior of the waveguide is shown in Figure 4.

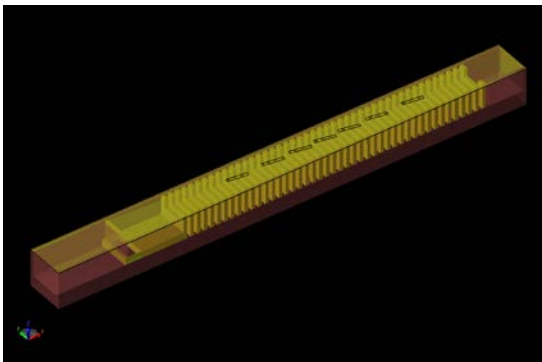


Figure 1: CAD view of the geometry constructed in XFDTD showing the CRLH waveguide and the radiating slots.

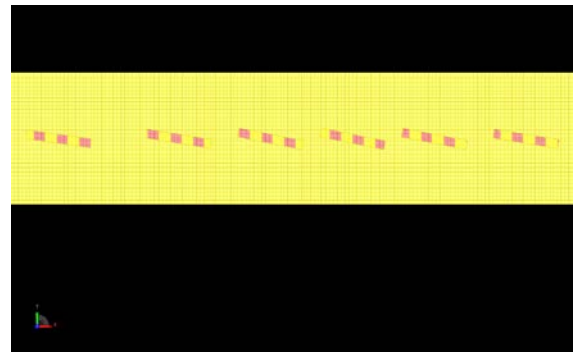


Figure 2: Detailed view of the XACT-meshed rotated slots of the device.

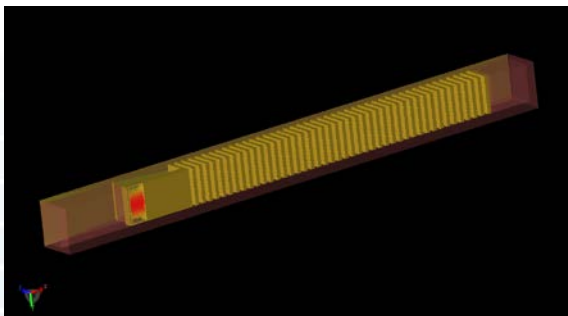


Figure 3: Bottom view of the device showing the input port with the waveguide excitation.

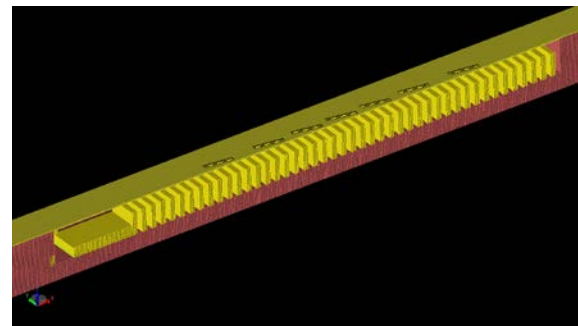


Figure 4: Cross-sectional mesh view of the device showing the interior CRLH cells.

Example 1: Slotted Waveguide Antenna

The geometry is meshed with large boundaries surrounding the structure for better display of color field images. As meshed, the geometry requires about 268 MB of memory to simulate and runs in slightly more than six minutes on an NVIDIA C1060 Tesla GPU card.

Of primary interest in this example is the resulting radiation pattern from the device. The three-dimensional gain pattern from the antenna at the center frequency of 10 GHz is shown in Figure 5 with the device at the center of the pattern. The gain in H- and E-planes is shown in Figures 6 and 7. The conduction currents along the top plate of the antenna are shown in Figure 8. In Figure 9 the transient electric field radiating out of the waveguide is shown at an instance in time.

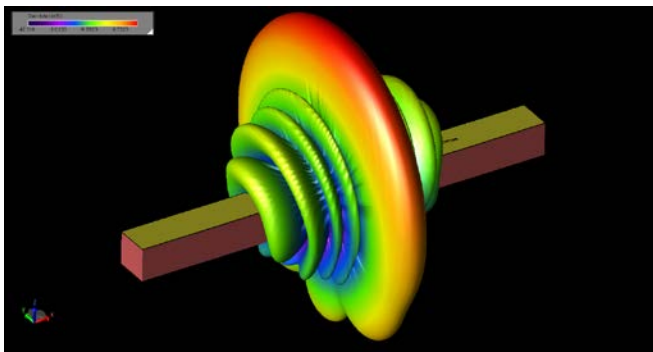


Figure 5: The three-dimensional radiation pattern of the antenna at 10 GHz.

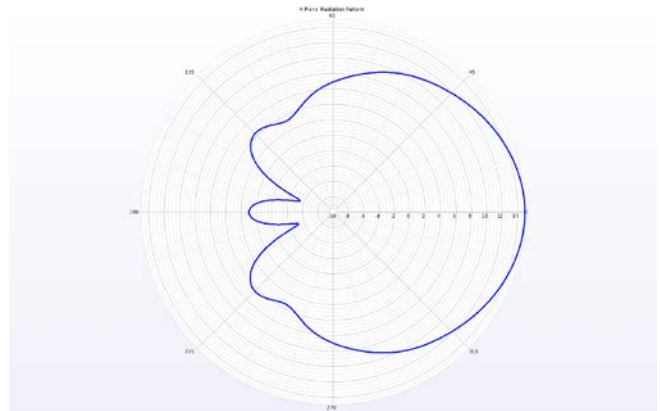


Figure 6: The H-plane radiation pattern at 10 GHz.

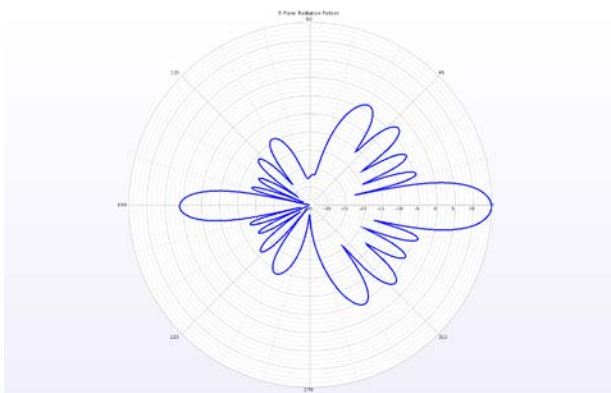


Figure 7: The E-plane radiation pattern at 10 GHz.

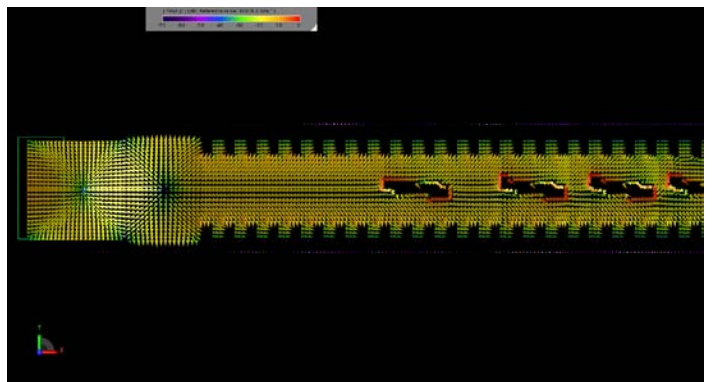


Figure 8: Vector display of the conduction currents on the top of the waveguide at 10 GHz.



Example 1: Slotted Waveguide Antenna

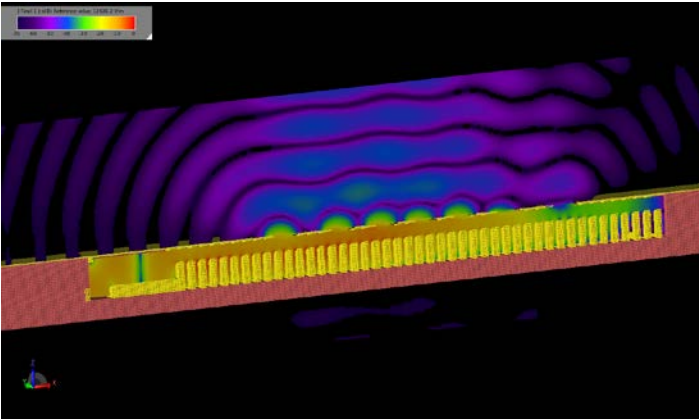


Figure 9: Image of the transient electric field in a cross-section of the device.

Request project files for this example by visiting:

<https://www.remcom.com/examples/slotted-waveguide-antenna.html>

References

1. S. Liao, J. Wang, Y. Chen, W. Tang, J. Wei, J. Xu, and Z. Zhao, "Synthesis, Simulation and Experiment of Unequally Spaced Resonant Slotted-Waveguide Antenna Arrays Based on the Infinite Wavelength Propagation Property of Composite Right/Left-Handed Waveguide," *IEEE Trans. Antenna Propag.*, Vol. 60, July 2012, pp. 3182-3194.



Example 2: Waveguide Cross-Coupled Filter Simulation

Summary: Waveguide ports are used to excite a complex microwave filter with a folded waveguide structure linked by a cross-coupled filter.

This example demonstrates the waveguide port source added with XFDTD in a complex structure of a cross-coupled filter [1]. The filter structure is comprised of a WR-90 waveguide that is folded in a tight curve with an aperture coupled-cavity at the bend of the curve. Several irises are inserted within the waveguide as well. Details of the design procedure are described in the paper.

In the XFDTD simulation, the structure is first created as a CAD model as shown in Figure 1. The yellow portion of the structure is the waveguide filter while the two green rectangles at the edges represent the locations of the waveguide ports. The structure is created based on a parameter list for each dimension defined in the paper and shown in Figure 2. A global mesh size of 0.5 mm is used for this simulation with XACT Accurate Cell Technology meshing applied to the curved waveguide portion and Fixed Points meshing used for the waveguide ports. This configuration results in a varying mesh size which places grid lines precisely at the edges of each geometry feature. A cross-section of the resulting mesh is shown in Figure 3.

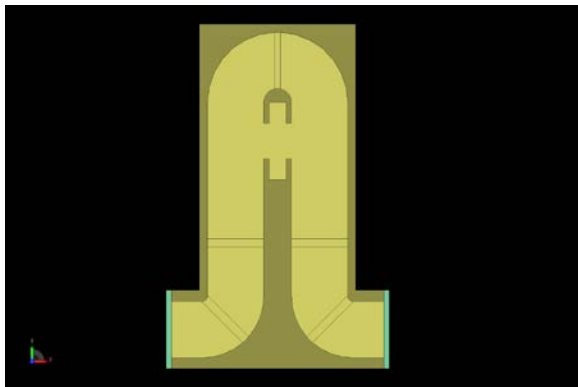


Figure 1: CAD representation of the waveguide cross-coupled filter geometry.

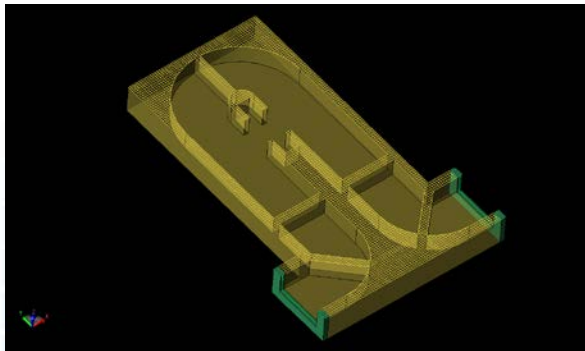


Figure 3: Cross-sectional view of the XFDTD mesh of the cross-coupled filter geometry.

Name	Formula	Value
CoupleOffset	0 mm	0
HouseThick	2 mm	0.002
LeadLength	7 mm	0.007
a	22.86 mm	0.02286
b	10.16 mm	0.01016
d	5 mm	0.005
d1	0.5 mm	0.0005
dist1	r3-B-12-11	-0.03581
l1	9.64 mm	0.00964
l2	21.57 mm	0.02157
l3	16.76 mm	0.01676
middle_iris_off	0.1 mm	0.0001
p1	6.40 mm	0.0064
p2	13.91 mm	0.01391
r1	11.16 mm	0.01116
r1interior	1 mm	0.001
r2	2.00 mm	0.002
r3	12.16 mm	0.01216
t1	1.00 mm	0.001
t2	1.50 mm	0.0015
timestep	4.92798e-13	4.92798220187...
w1	15.07 mm	0.01507
w2	12.40 mm	0.0124
w3	9.25 mm	0.00925

Figure 2: XFDTD parameter list of all dimensions used in the cross-coupled filter geometry.

Example 2: Waveguide Cross-Coupled Filter Simulation

The ports are added across the openings of the waveguide and the distribution is set up as a TE₁₀ mode, as shown in Figure 4 for the input port. The simulation is executed with an input waveform with frequency content over the 8-12 GHz range of the device. The time to complete the example to -45dB convergence is about 15 minutes on an NVIDIA C1060 Tesla GPU card. Following the simulation, the S-Parameters at the input and output ports are available and are displayed in Figure 5.

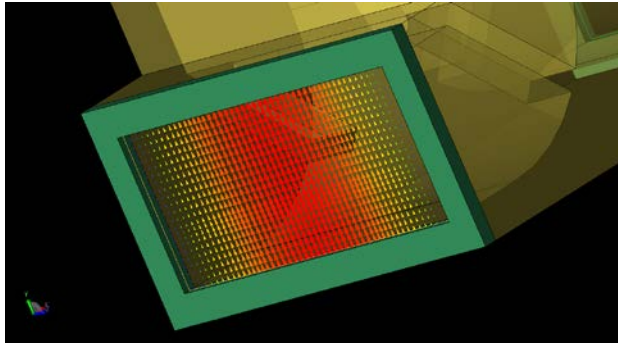


Figure 4: The TE₁₀ waveguide port excitation applied to the input port of the device.

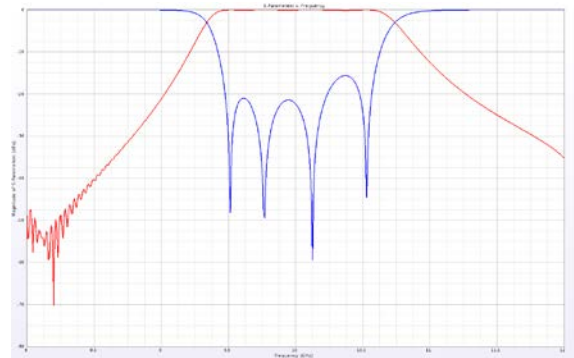


Figure 5: The computed S₁₁ and S₂₁ of the cross-coupled filter geometry.

Request project files for this example by visiting:

<https://www.remcom.com/examples/waveguide-cross-coupled-filter-simulation.html>

References

1. Q. F. Zhang and Y. L. Lu, "Dimensional Synthesis of Symmetric Wideband Waveguide Cross-Coupled Filters Without Global Full-Wave Optimization," *IEEE Trans. Microw. Theory Tech.*, vol. 58, pp. 3742-3748, Dec. 2010.



Example 3: Wideband Pseudo-Elliptic Waveguide Filter

Summary: Waveguide ports are used to excite a microwave filter constructed from a WR-90 waveguide with cavity-backed inverters and multiple irises.

This example describes the simulation of a waveguide filter that includes both E- and H-plane cavity-backed inverters in addition to several irises [1]. The basic geometry is shown in CAD format in Figure 1 where the E-plane cavity-backed inverter is above the waveguide and the H-plane cavity-backed inverter is on the back side. The waveguide is WR-90 and the dimensions of the design including the spacing and dimensions of the cavities and irises are easily entered as parameters into the XFDTD model. The structure is meshed with a 0.4 mm base cell size and fixed points are used on all parts to ensure the FDTD grid lines overlap the CAD dimensions.

The input port has a fundamental mode applied as shown in the cut-away mesh view of Figure 2. The frequency for the input excitation is 12 GHz which ensures frequency content in the simulation over the 8 to 12 GHz range of the device. The output for the simulation will be the S-parameters at the input and output ports, some images of the transient electric field propagation through the device, and point sensors of the electric field versus time.

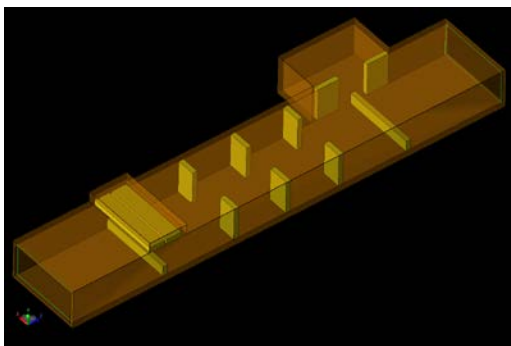


Figure 1: CAD representation of the device as constructed in XFDTD.

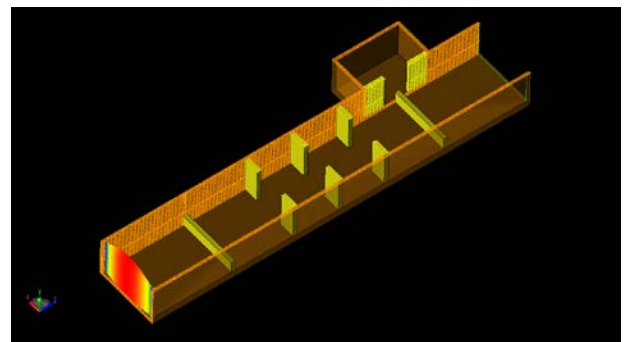


Figure 2: Cross-sectional XFDTD mesh view of the device with the input port excitation displayed.

The simulation requires approximately 122 MB of computer memory and runs to -45dB convergence in just over 14 minutes on an NVIDIA C1060 Tesla GPU card.

Following the simulation, the resulting S-parameters at each port, shown in Figure 3, are found to be a good match to the measured values reported in the paper. The transient electric field at an instance in time through the cross-section of the filter is shown in Figure 4. The transient electric field at point locations centered just beside each of the ports is shown in Figure 5.

Example 3: Wideband Pseudo-Elliptic Waveguide Filter

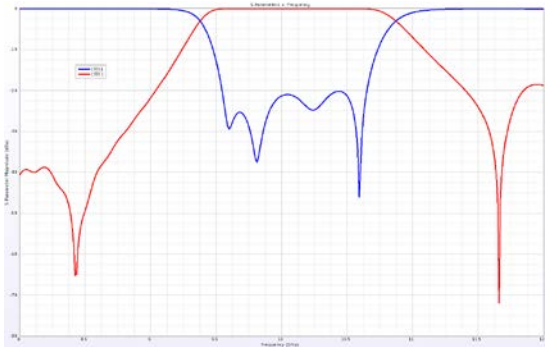


Figure 3: Resulting S_{11} and S_{21} of the device as simulated in XFDTD.

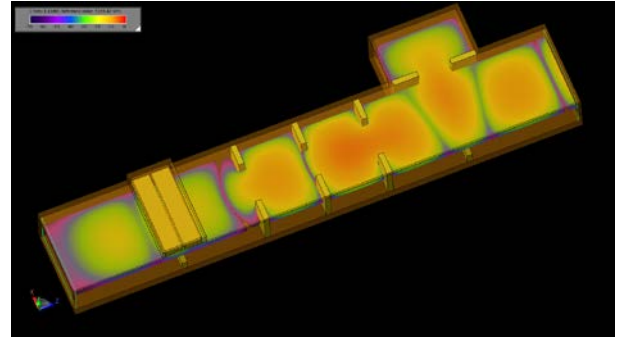


Figure 4: Transient electric fields propagating in the filter.

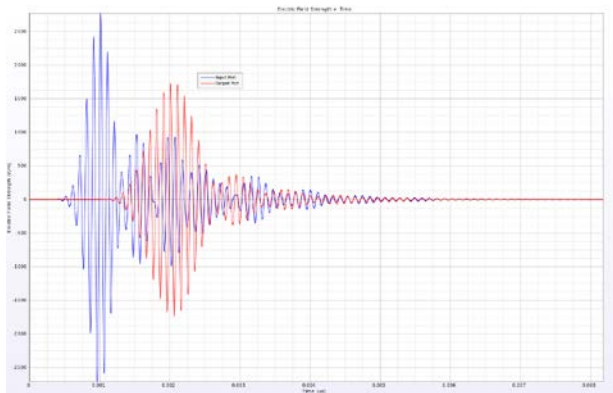


Figure 5: Electric field point sensor at the input and output ports of the filter.

Request project files for this example by visiting:

<https://www.remcom.com/examples/2017/3/27/wideband-pseudo-elliptic-waveguide-filter>

References

1. Q. F. Zhang and Y. L. Lu, "Design of Wide-Band Pseudo-Elliptic Waveguide Filters With Cavity-Backed Inverters," *IEEE Microw. and Wirel. Comps. Letters*, vol. 20, pp. 604-606, Nov. 2010.



Example 4: Rectangular Waveguide Mode Converters

Summary: This example investigates higher order modes available in waveguide ports in XFDTD. Here rectangular waveguides of WR187 size (47.55 x 22.15 mm) are used to create mode converters by introducing double or triple bends.

This example investigates higher order modes available in waveguide ports in XFDTD. Here rectangular waveguides of WR187 size (47.55 x 22.15 mm) are used to create mode converters by introducing double or triple bends. The structures for this example come from a journal paper [1].

The first device considered is a dual bend mode converter shown in Figure 1. Here, two straight waveguide sections are connected to a center part that has two bends to form a partial "S" shape with the function of converting a TE₁₀ mode to TE₂₀ or vice versa. The device is constructed as a CAD model in XFDTD and then meshed in the software using the XACT Accurate Cell Technology conformal meshing feature to accurately describe the curvature of the waveguide. A cross-sectional view of the mesh is shown in Figure 2 where a base mesh size of 1 mm is used.

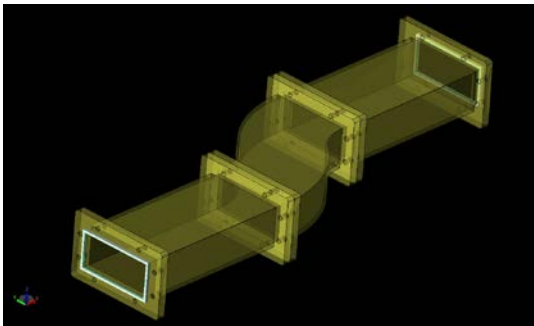


Figure 1: CAD geometry of the dual bend waveguide mode converter.

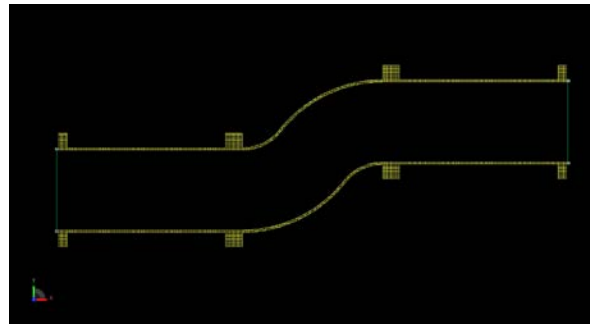


Figure 2: Cross sectional view of the XFDTD mesh of the dual bend geometry.

The simulation is performed with an input waveform with frequency content from 8-10 GHz with a TE₁₀ mode active to create a TE₂₀ mode at the output. The calculation is run on an NVIDIA Tesla C1060 GPU card and execution time is just over three minutes. Slightly more than 100 MB of memory are required.

Following the simulation, the steady state electric fields in the device are displayed at 8.5 GHz (Figure 3) to show the mode conversion that takes place in the double bend section of the waveguide. The steady state fields at the input and output ports are displayed in the angled view of Figure 4. The electric field in a line across the width of the output port is then plotted and compared to measured results from the paper [1] with very good agreement (Figure 5).



Example 4: Rectangular Waveguide Mode Converters

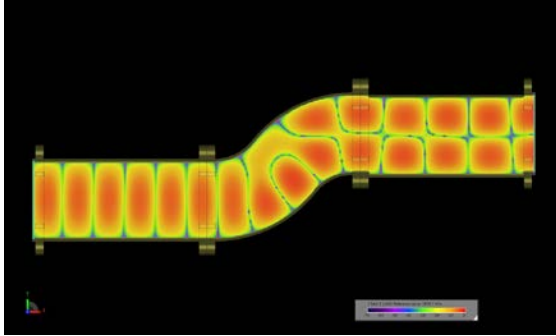


Figure 3: The steady-state electric field distribution in the dual bend converter at 8.5 GHz.

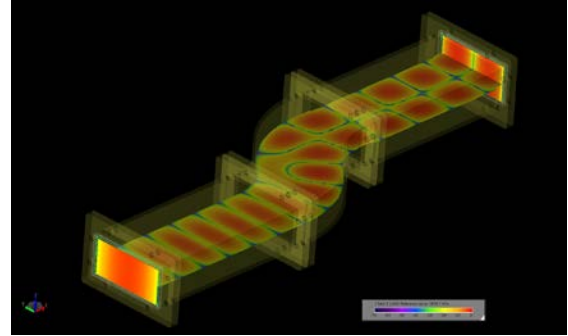


Figure 4: The steady-state electric field distribution in the dual bend converter at 8.5 GHz with the field distribution at each of the ports displayed.

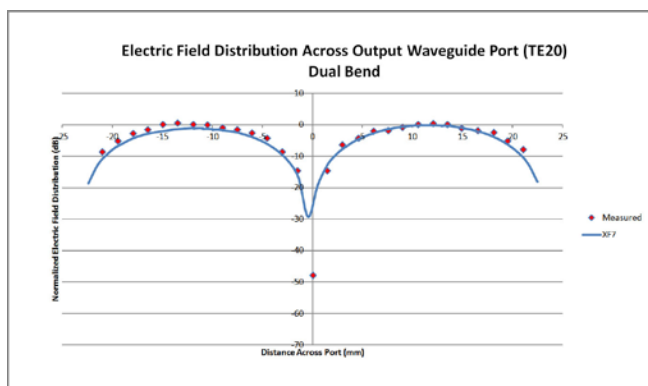


Figure 5: Comparison plot of the XFdtd electric field distribution across the dual bend converter waveguide port and measurements.

A second mode converter is created in a similar manner except in this case three bends are introduced into a section of waveguide, as shown in Figure 6. This device is meshed in the software with a 1 mm base cell size and the XACT feature. The resulting mesh is shown in a cross-sectional view in Figure 7. A TE₁₀ mode is applied at the input port and the output TE₂₀ mode is captured. The calculation is performed in just over two minutes in about 88 MB of memory. The resulting steady state electric fields at the port ends and through the center of the waveguide may be seen in Figure 8. The electric field across the output port is plotted versus measurements and again the agreement is very good as shown in Figure 9.

Example 4: Rectangular Waveguide Mode Converters

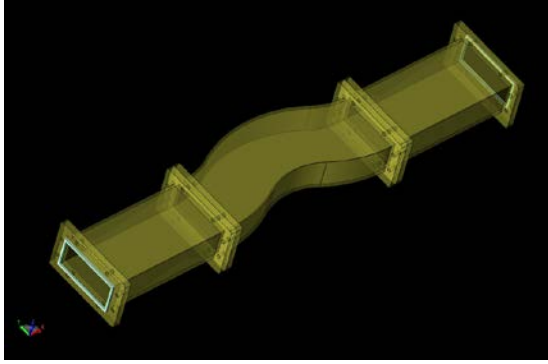


Figure 6: CAD geometry of the tri-bend waveguide mode converter.

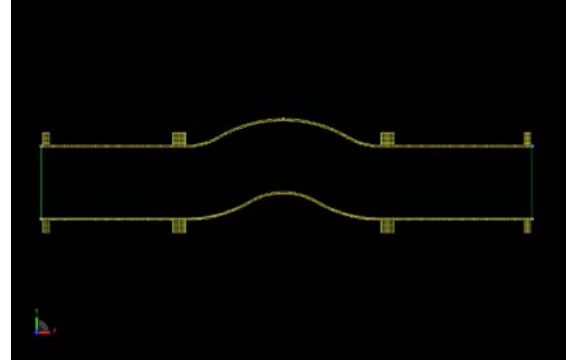


Figure 7: Cross sectional view of the XFDTD mesh of the tri-bend geometry.

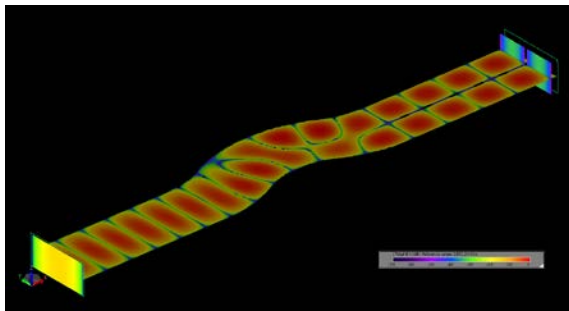


Figure 8: The steady-state electric field distribution at the ports and inside the tri-bend mode converter at 8.5 GHz.

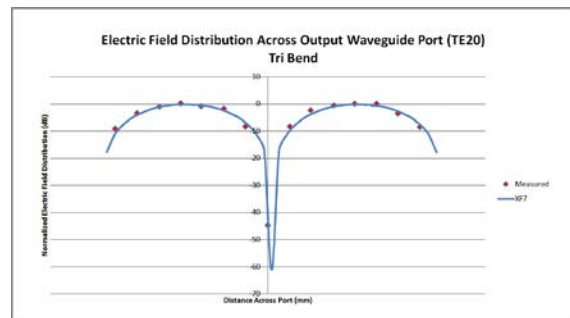


Figure 9: Comparison plot of the XFDTD electric field distribution across the tri-bend converter waveguide port and measurements.

As a final exercise, a combination of the previous mode converters is constructed to form a TE40 to TE10 device which is shown in Figures 10 and 11. The larger TE40 side connects to two tri-bend mode converters which are mirror imaged and produce an effect of putting the TE40 mode into TE20 form. An exponentially-tapered region is then added to reduce the waveguide size from two WR187 guides to a single WR187 which then feeds into a dual bend mode converter. The output of the dual bend converter is a TE10 mode.

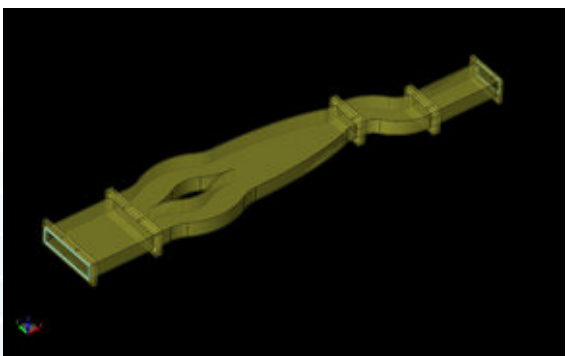


Figure 10: CAD geometry for the multi-mode converter shown in an angled view.

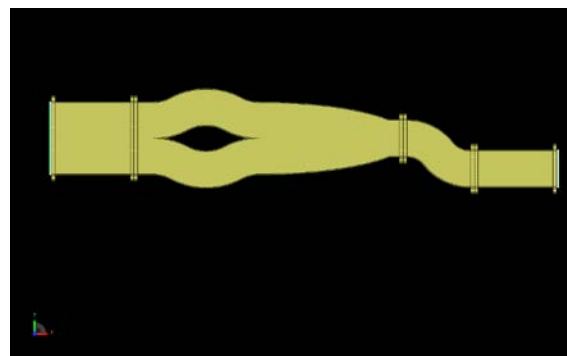


Figure 11: CAD geometry for the multi-mode converter shown in a cross-sectional view.



Example 4: Rectangular Waveguide Mode Converters

The simulation is performed with an 8.5 GHz sinusoidal input with the TE₄₀ mode active and the output collected at the TE₁₀ port. On an NVIDIA Tesla C1060 GPU card, the simulation converges to a -40dB level in approximately one and a half minutes using 274 MB of memory. The propagation of the TE₄₀ mode into the output TE₁₀ mode is shown in the transient field images of Figures 12 through 15 where each of the intermediate steps is also visible. The steady state electric field distribution in the waveguide and at the two ports is shown in Figure 16. The resulting electric field distribution across the output port is then shown in Figure 17.

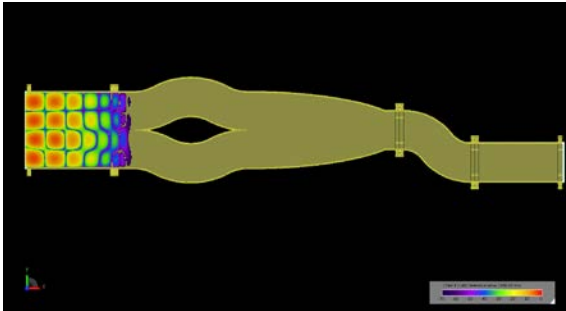


Figure 12: Transient electric field propagation in the multi-mode converter as the TE₄₀ fields reach the entrance to the dual tri-bend converters.

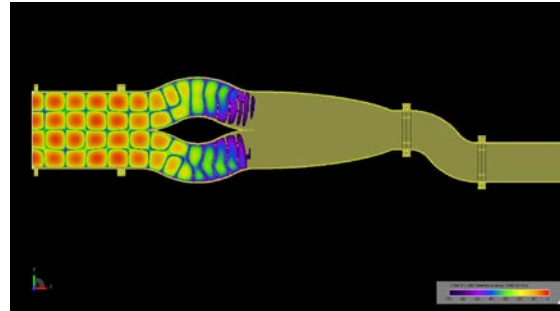


Figure 13: Transient electric field propagation in the multi-mode converter as the TE₄₀ fields are converted to TE₂₀ by the dual tri-bend converters.

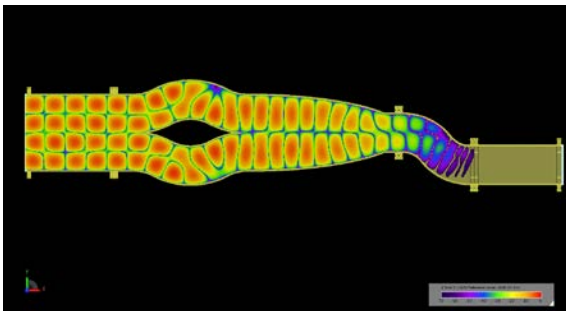


Figure 14: Transient electric field propagation in the multi-mode converter as the TE₂₀ fields pass through the dual bend mode converter and are transformed to TE₁₀.

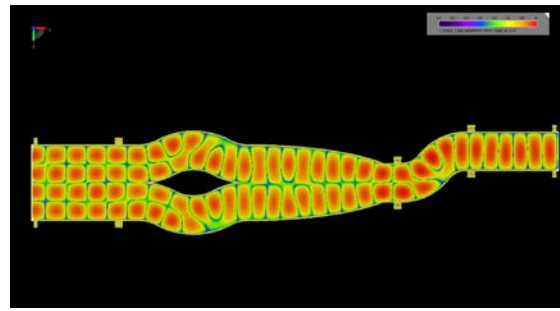


Figure 15: Transient electric field propagation in the multi-mode converter showing the complete path of the TE₄₀ fields through the tri-bend and dual bend mode converters to the output port where they emerge as TE₁₀.

Example 4: Rectangular Waveguide Mode Converters

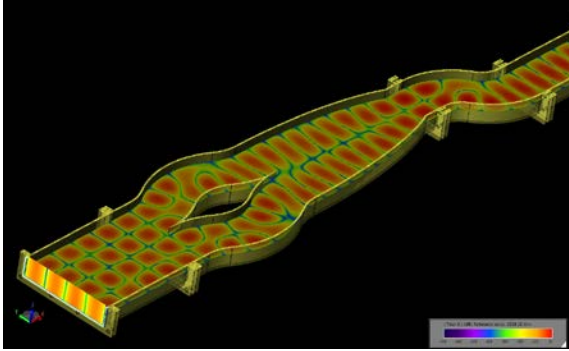


Figure 16: The steady-state electric field distribution at the ports and inside the multi-mode converter at 8.5 GHz.

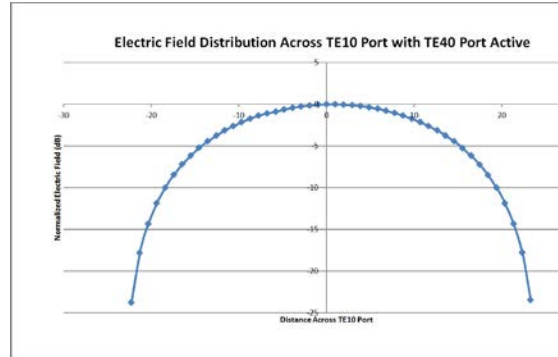


Figure 17: Plot of the XFDTD electric field distribution across the TE10 port of the multi-mode converter with the TE40 port active.

Request project files for this example by visiting:

<https://www.remcom.com/examples/rectangular-waveguide-mode-converters.html>

References

1. Q. Zhang, C. W. Yuan, and L. Liu, "Theoretical Design and Analysis for TE20-TE10 Rectangular Waveguide Mode Converters," *IEEE Trans. Microw. Theory Tech.*, Vol. 60 no. 4, Apr. 2012, pp. 1018-1026.



Example 5: Microstrip Gap Waveguide on Electronic Band Gap Substrate

Summary: A microstrip gap waveguide is simulated over a mushroom-type electronic band gap (EBG) surface to demonstrate the effectiveness of the design.

A microstrip gap waveguide is simulated over a mushroom-type electronic band gap (EBG) surface to demonstrate the effectiveness of the design. The simulations shown in this example are taken from a design in the referenced paper [1].

The device operates in the 5-12 GHz range and consists of a mushroom-type EBG substrate with a trace inserted between two walls. The entire device is enclosed in a metal box with the only openings via the two ports at each end. Views of the geometry in CAD format are shown in Figures 1 and 2 where the top of the box has been made invisible to show the interior details. The device is designed so that propagation takes place in the air region between the mushrooms and the top of the box. As the width of the air region is only one millimeter, a fairly small FDTD mesh size of 0.2 mm is used to provide enough resolution for the fields. A three-dimensional view of the mesh near one of the ports is shown in Figure 3 where the display of the metal box and the dielectric substrate is disabled to show the details. The XACT meshing feature is used for the EBG and microstrip parts of the geometry to accurately mesh the curves and edges.

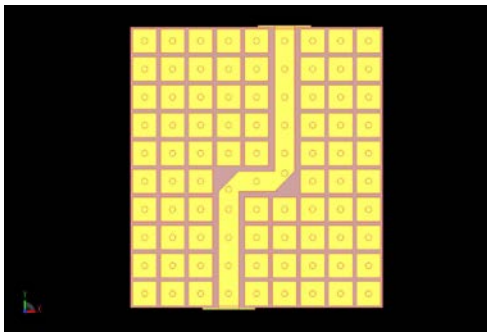


Figure 1: A CAD rendering of the geometry shown from the top. Here the lid of the metal box containing the device has been removed to reveal the contents of the interior.

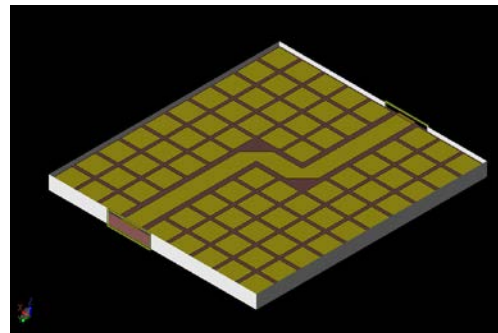


Figure 2: A CAD view of the geometry shown at an angle with the top of the box removed.

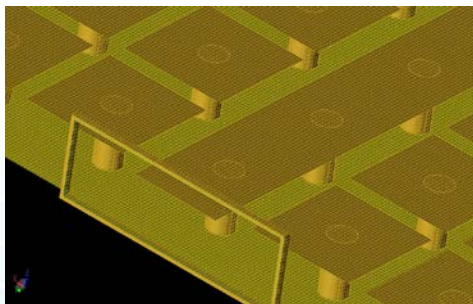


Figure 3: A three-dimensional view of the XFtd mesh of the device near one of the ports. The box and substrate have been removed in this view to show the interior detail.

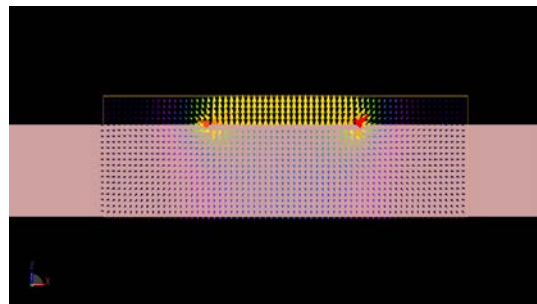


Figure 4: The field pattern of the input excitation at port 1 where the fields are shown to be primarily between the microstrip line and the metal cover.



Example 5: Microstrip Gap Waveguide on Electronic Band Gap Substrate

The device is excited by TEM waveguide ports attached to each end of the microstrip line. The excitation, shown in Figure 4, is applied with a frequency-limited signal with content from about 5 to 12 GHz to one of the ports. S-parameter and field image data is saved as output.

The calculation is executed on an NVIDIA Tesla C1060 GPU card in approximately 39 minutes while using about 206 MB of memory. The calculation takes a fairly long time to converge due to resonant fields in the box which decay slowly.

Following the simulation, the computed S-parameters can be compared to measured data presented in the paper [1]. In Figures 5 and 6 the S11 and S21 results are plotted, respectively, against the measured data and show similar results. The steady state electric field distribution at 9 GHz in the middle of the air region above the EBG surface is plotted in Figure 7. Here it can be seen that the fields are contained in the region above the microstrip line as expected. Finally, the steady state conduction currents on the EBG surface are plotted at 9 GHz and are shown in Figure 8 and again the field strength can be seen to drop off significantly away from the microstrip line.

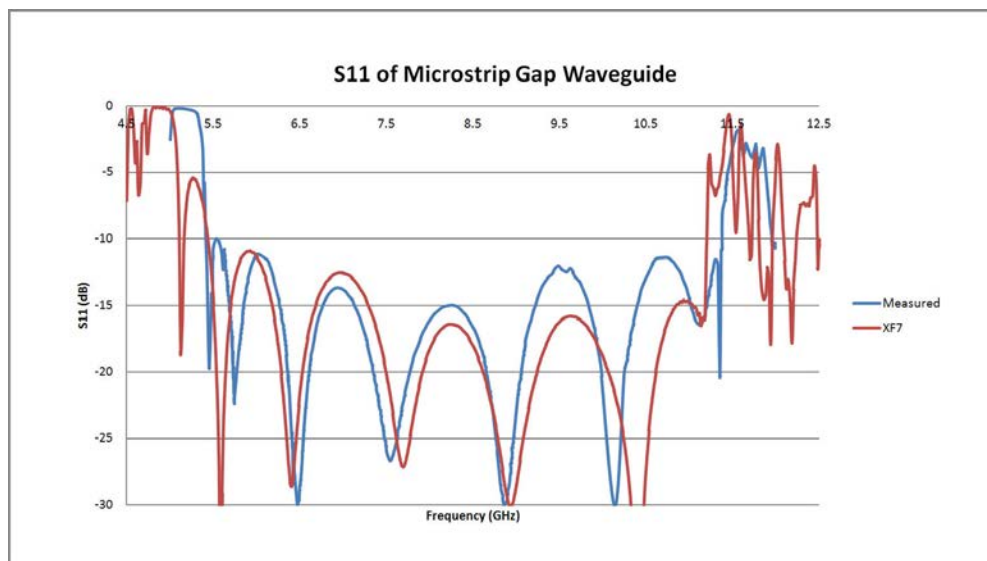


Figure 5: A comparison of the return loss (S11) of the device as simulated in XFDTD shown with measured data.



Example 5: Microstrip Gap Waveguide on Electronic Band Gap Substrate

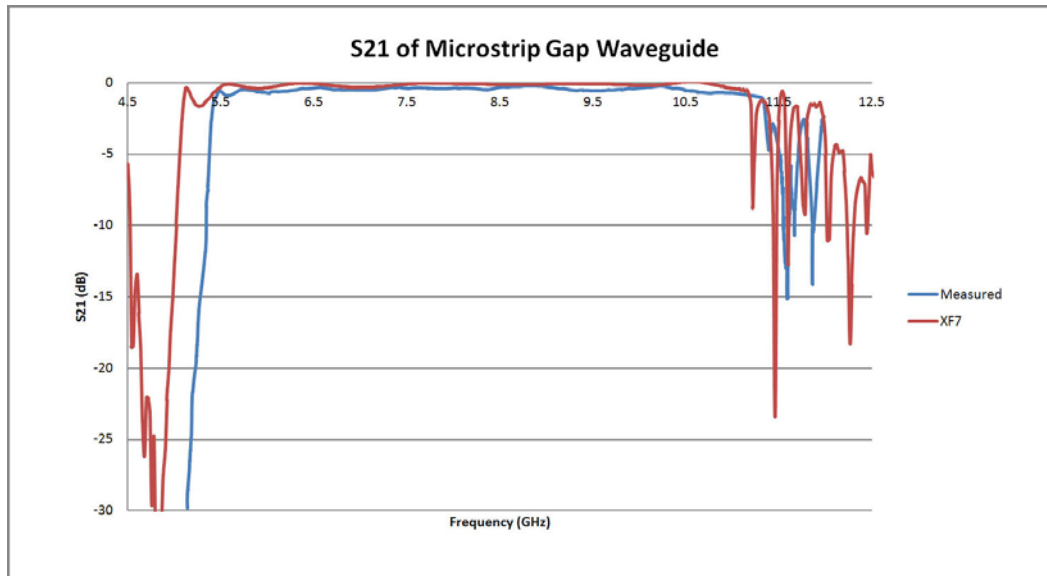


Figure 6: A comparison of S_{21} of the device between the simulated XFDTD results and measurements.

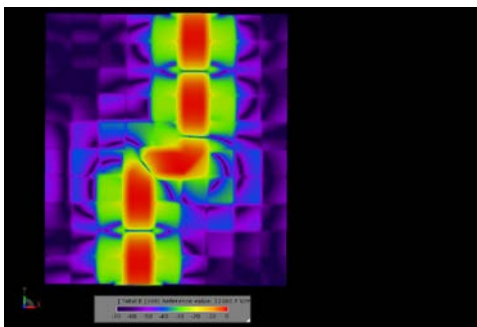


Figure 7: The steady state electric field distribution at 9 GHz in the center of the air region between the EBG surface and the metal lid of the box. The fields are shown to be tightly constrained to the microstrip region.

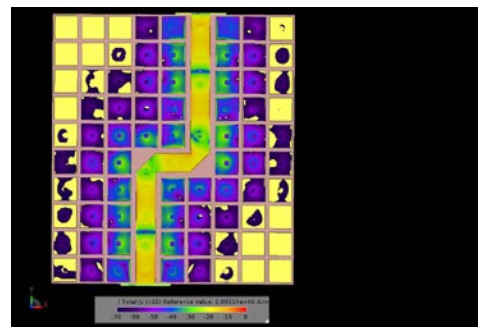


Figure 8: The steady state conduction currents on the top of the EBG surface. The currents are bound tightly to the microstrip region.

Request project files for this example by clicking here:

<https://www.remcom.com/examples/microstrip-gap-waveguide-on-electronic-band-gap-substrate.html>

References

1. E. Pucci, E. Rajo-Iglesias, P. S. Kildal, "New Microstrip Gap Waveguide on Mushroom-Type EBG for Packaging of Microwave Components," *IEEE Microw. Wireless Compon. Letters*, Vol. 22, No. 3, Mar. 2012, pp. 129-131.

